The Strength of the OH-Bend/OH-Stretch Fermi Resonance in Small Water Clusters

Main Supplement

Nils O. B. Lüttschwager

February 20, 2024

Jupyter notebooks are published together with this supplement and will be referenced *via* the token *NB* plus the notebook number and, optionally, the number of a particular section. For example, *NB/1/4* is a reference to the notebook `1_cluster-integrals.ipynb`, Section 4 *Run Integration*. PDF exports of the notebooks are available for convenience, but we note that there are some shortcomings in the formatting, e.g. for the syntax-highlighting in code blocks where some regular words are being interpreted as keywords and displayed in bold font, or not all special characters being displayed correctly.

1 Measurement Conditions

Measurement conditions are summarized in Table S1. For an explanation of the spectrum labels, see Section 3 of the main paper.

To estimate the flow through the nozzle, we used the following equation from Ref. 1:

$$\dot{V}_s = A \, \frac{p_0}{p_s} \left(\frac{p_{\text{crit}}}{p_0} \right)^{\frac{1}{\kappa}} \sqrt{\frac{2\kappa}{\kappa - 1} \frac{RT_0}{M} \left[1 - \left(\frac{p_{\text{crit}}}{p_0} \right)^{\frac{\kappa - 1}{\kappa}} \right]}$$

A is the nozzle area (slit length 4 mm × slit width 0.15 mm), p_0 the stagnation pressure (at nozzle, before expansion), p_s the standard pressure (1.0 bar), $p_{\text{crit}} = p_0 \left(\frac{2}{\kappa+1} \right)^{\frac{\kappa}{\kappa-1}}$ the critical pressure at which the expansion becomes supersonic, κ the heat capacity ratio (≈ 1.67 for a monoatomic ideal gas), T_0 the temperature of the gas prior to expansion, and M its molar mass.

Table S1: Measurement conditions; p_0 – stagnation pressure at nozzle input, p_b – background pressure in vacuum chamber, d – distance from nozzle exit (slit) to laser, G – number of grooves per millimeter of the used grating, P – optical laser power.

label	carrier gas	p_0/mbar	p_b/mbar	d/mm	G/mm^{-1}	P/W	scans (overall exposure)
He/600/1/hr	He	600	11	1.0	1312	15	24 × 300 s (2 h)
He/600/2/hr	He	600	11	2.0	1312	15	144 × 300 s (12 h)
Ne/200/2/hr	Ne	200	3	2.0	1312	18	133 × 300 s (11.1 h)
Ne/300/2.5/hr	Ne	300	4	2.5	1312	15	180 × 300 s (15 h)
NeAr/400/0.75/hr	Ne + 10% Ar	410	5	0.75	1312	18	24 × 300 s (2 h)
NeAr/400/1/hr	Ne + 10% Ar	410	5	1.0	1312	18	15 × 300 s (1.3 h)
NeAr/400/2/hr	Ne + 10% Ar	410	5	2.0	1312	18	99 × 300 s (8.3 h)
NeAr/400/2.5/hr	Ne + 10% Ar	410	5	2.5	1312	18	90 × 300 s (7.5 h)
He/600/1/lr	He	605	11	1.0	500	18	44 × 180 s (2.2 h)
He/600/1.5/lr	He	605	11	1.5	500	18	38 × 300 s (3.2 h)
He/600/2a/lr	He	605	11	2.0	500	18	48 × 300 s (4 h)
He/600/2b/lr_l	He	600	10 to 11	2.0	500	18	58 × 300 s (4.8 h)
He/600/2b/lr_m	He	600	10 to 11	2.0	500	18	114 × 300 s (9.5 h)
He/600/2b/lr_h	He	600	10 to 11	2.0	500	18	176 × 300 s (14.7 h)
He/600/2c/lr_l	He	600	11	2.0	500	18	75 × 900 s (18.8 h)
He/600/2c/lr_h	He	600	11	2.0	500	18	63 × 900 s (15.8 h)

2 Raw Data Processing

Raw data processing is done in NB/0 and most information on the process is given there. One exception is the scaling of Raman intensities to account for the frequency dependence of the Raman scattering cross-section. The Raman scattering cross-section depends on the laser wavenumber (index L) and Raman shift (index R) as follows:[2]

$$\sigma' \propto \frac{(\tilde{\nu}_\mathrm{L} - \tilde{\nu}_\mathrm{R})^3 \tilde{\nu}_\mathrm{L}}{\tilde{\nu}_\mathrm{R}} = C(\tilde{\nu}_\mathrm{R}) \tag{1}$$

There is also a Boltzmann term, but under jet-cooled conditions it is very close to 1 for the observed vibrations which fall in the range 3100 cm^{-1} to 3700 cm^{-1} and can be neglected. With the laser wavelength close to 532 nm ($\approx$ 18 800 cm^{-1}), Equation 1 yields that transitions at 3100 cm^{-1} scatter light about 34 % more strongly than those at 3700 cm^{-1}. This effect needs to be corrected if one wants to compare transition moments quantitatively, like it is done in the Fermi resonance analysis presented in this work. The effect is corrected by scaling intensities—photoelectrons per second per reciprocal centimeter—by $C(3152\,\mathrm{cm}^{-1})/C(\tilde{\nu}_\mathrm{R})$ (Equation 1). The constant factor $C(3152\,\mathrm{cm}^{-1})$ is introduced so that the overall intensity scaling is equal to 1 at 3152 cm^{-1}, the band center of the monomer OH bending overtone. In doing this, the information about how many photons per time and spectral bandwidth were detected is

largely retained while relating intensities to transition moments in a quantitative way becomes possible.

3 Correction of Experimental Intensities

Vignetting—Spectra recorded with the cookie-jet suffer from vignetting close to the low-frequency side of the CCD detector. This is visible in raw spectra (NB/0) and in particular in spectra recorded from a continuous calibration lamp (NB/0.1), but concerns only spectra recorded with the high resolution grating, where overtone ro-vibrational lines (monomer) and the overtone band (clusters) may be attenuated, while for the lower resolution grating the interesting signals with the smallest wavenumbers are positioned in the center of the CCD detector and thus are not attenuated. We tried to quantify this attenuation but found a different onset of vignetting, depending on how we illuminated with the calibration lamp. The strongest vignetting that we found would start at pixel ≈ 120 or about $3190\,\mathrm{cm}^{-1}$ for the high resolution measurements, but other measurements had onsets rather around pixel ≈ 50 (NB/0.1/6). Thus, we could correct for vignetting only with considerable uncertainty. To account for this uncertainty, we included the vignette correction in our Monte-Carlo based integration of Raman bands, where for each Monte-Carlo draw, a random spline fit that falls between the most strongly and least strongly attenuated sensitivity measurements is used to apply a vignette correction (NB/0.1/7). The spline fit yields the sensitivity at each pixel as a percentage value by which the intensity at that pixel is divided to apply the correction. Since the overtone band falls only barely in the potentially attenuated spectral region, the effect on cluster integrals is insignificant (NB/1/6). However, the effect on integrals from monomer ro-vibrational lines, which clearly fall in the attenuated region, is rather significant and responsible for about half the uncertainty in the coupling constants derived from high resolution measurements (NB/2). Since the ro-vibrational lines are quite narrow, we applied the vignette correction in a simpler way: the integrals of the lines at 3152 and $3159\,\mathrm{cm}^{-1}$ where divided by an uncertain factor with a uniform distribution in the range [0.7, 0.9] and [0.75, 1.0], respectively (NB/2/3.1), *i.e.* the potential range of the sensitivity we found in NB/0.1/6 at the positions of these lines.

Polarization Dependence—In general, a grating spectrograph shows a different sensitivity towards light polarized parallel or perpendicular to the grooves of the grating, and this sensitivity strongly depends on the particular grating and wavelength. Since we detect light without a polarizing filter, *i.e.* unspecific with regards to its polarization direction (to retain maximum signal), the intensity ratio of two bands with different depolarization ratios is not directly comparable to transitions moments and will likely vary when measured with different gratings. If

the depolarization ratio is known or can be estimated from quantum chemical calculations, it is possible to correct for this effect,[3] but for the overtone band in this work, this is not the case. We addressed this issue by measuring the sensitivity of the setup for the two gratings as a function of polarization and wavelength using a polarizing filter in front of the spectrograph, turned to maximize or minimize the signal of the continuous calibration lamp. By doing this, we found a difference in sensitivity by a factor of ~ 0.7 for the $1312\,\mathrm{g\,mm^{-1}}$ grating and ~ 0.8 for the $500\,\mathrm{g\,mm^{-1}}$ grating in the spectral region of interest (NB/0.1/8). When adjusting the setup for maximum Raman sensitivity, we measure nitrogen and turn the $\lambda/2$ plate in the laser beam path to maximize the Q-branch intensity at $\sim 2330\,\mathrm{cm^{-1}}$. Since the nitrogen Q-branch is strongly polarized, polarized Raman bands will in general have a polarization direction that is close to optimal with regards to the sensitivity of the spectrograph. The repolarized part of the Raman scattered light, however, will be attenuated, roughly by the factors of 0.7 and 0.8 that we found for the high resolution and low resolution grating, respectively. If we assume a maximum depolarization ratio of 0.75, we find the sensitivity ratio of depolarized to polarized Raman signals to be:

$$\begin{aligned} I(f) &= I_{\perp} \times f + I_{||} \\ I(f) &= 0.75 I_{||} \times f + I_{||} \\ I(f) &= I_{||}\,(0.75 f + 1) \\ \text{sensitivity ratio} &= \frac{I(f)}{I(f=1)} = \frac{0.75 f + 1}{1.75} \end{aligned}$$

where f is the ratio of the sensitivity towards light polarized perpendicular and parallel with respect to the laser polarization plane. For $f = 0.7 \rightarrow$ sensitivity ratio $= 87\,\%$ while for $f = 0.8 \rightarrow$ sensitivity ratio $= 91\,\%$, which we round to $90\,\%$ and conclude that a Raman signal of unknown depolarization ratio could be attenuated by up to $10\,\%$. For unperturbed concerted OH stretch fundamental bands, we assume that the depolarization ratio is very close to zero, following the calculations from Cybulski and Sadlej,[4] so the polarization of the light will not lead to an attenuation (assuming that the Q-branch dominates the jet spectra). For the overtone band and some of the ro-vibrational lines of the monomer (3196, 3222, $3265\,\mathrm{cm^{-1}}$), we do not know the depolarization ratio and thus assume the maximum (uncertain) attenuation by $10\,\%$. We do the same for the fundamental bands of the tetramer and pentamer, since the corresponding states could have considerable overtone character. Similar as we did for correcting ro-vibrational line integrals for vignetting, we thus divide line and band integrals of the said signals by an uncertain factor with a uniform distribution in the range [0.9, 1.0].

4 Low Resolution Spectra

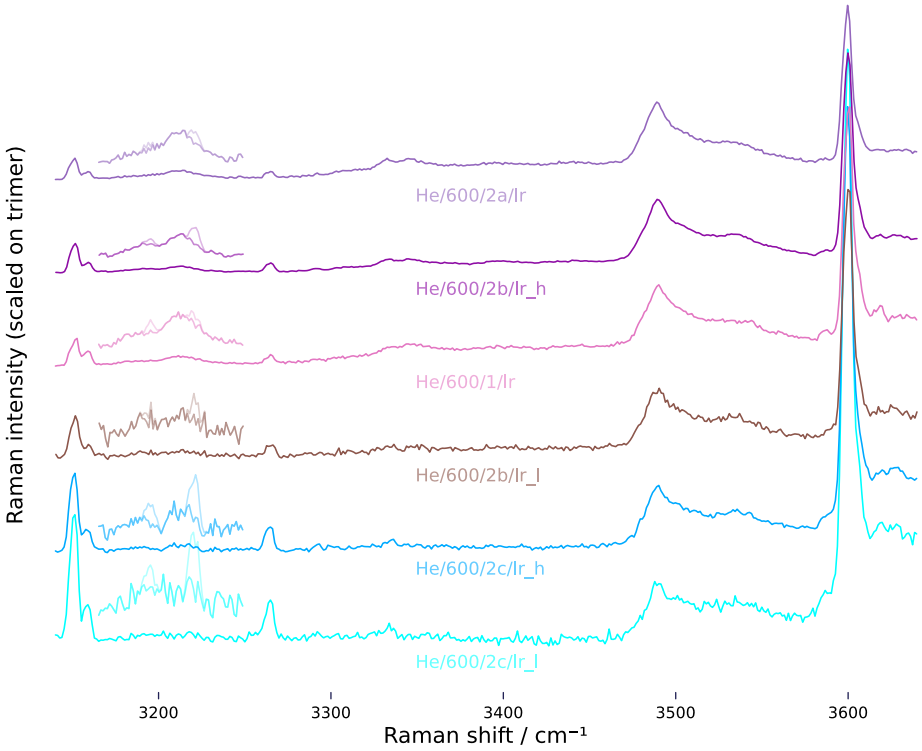

Figure S1: Raman jet spectra of water clusters measured under varying conditions using the 500 g mm^{-1} grating. The labeling scheme is *carrier gas/stagnation pressure in mbar/nozzle distance in mm/lr* for low resolution, see first paragraph of Section 3 in the main paper. Table S1 lists further measurement conditions. For better visibility, the overtone band is magnified by a factor 4. Ro-vibrational lines of the water monomer that overlap with the overtone band were removed by fitting Gaussian peak functions and are drawn with fainter colors.

5 Brute-Force Sampling

The "brute-force" approach used to derive coupling constants works as follows: For a set of trial coupling constants $W = \{W_2, W_3, W_4, W_5\}$ and band separations, the associated intensity ratio $R_n(W_n)$ is calculated for all cluster sizes n. Multiplying the intensity ratio with the measured area of the stretching fundamental band $A_{f,n}$ gives the overtone band integral for a particular cluster size. Adding up the contributions from all cluster sizes, a prediction (indicated by the tick) for the overall overtone band integral, A'_o, is derived:

$$A'_o = \sum_n R_n(W_n) A_{f,n} \tag{2}$$

This predicted band integral is compared to the measured band integral A_o. Since uncertainties are available for both, predicted and measured overtone band integral, it is possible to calculate a ζ-score:[5]

$$\zeta_{A_o} = \frac{|A'_o - A_o|}{\sqrt{u^2(A'_o) + u^2(A_o)}} \tag{3}$$

The ζ-score is a measure of agreement of two quantities. Values $\zeta > 2$ are an indication that one or both of the uncertainties are underestimated and may point at a problem with the underlying model(s)—like in our case, a poorly fitting coupling constant. Assuming normal distributions, a probability $p(\zeta)$ can be calculated on how likely it is that a particular ζ-score is observed if the difference $|A'_o - A_o|$ is due to random errors:

$$p(\zeta) = 1.0 - \mathrm{erf}\left(\zeta/\sqrt{2}\right) \tag{4}$$

Probabilities are calculated for all spectra and are combined by multiplication, giving an overall probability for each set of proposed coupling constants, $p(W)$. Finding a best guess is achieved by drawing values of W_2 to W_5 randomly with uniform probability in a physically meaningful interval, with a lower bound of $0\,\mathrm{cm}^{-1}$ and an upper bound of half the band distance or $100\,\mathrm{cm}^{-1}$, if the latter is smaller ($100\,\mathrm{cm}^{-1}$ is the upper cut-off value). Similarly, fundamental band integrals are drawn from normal distributions which are derived from the mean and standard deviation of the band integrals estimated by integration with *NoisySignalIntegration.jl*. The overtone band integral is predicted and its corresponding overall probability is calculated. For each cluster size, this probability is added to the "bin" (width $1\,\mathrm{cm}^{-1}$) for a particular value of the coupling constant. For example, if an iteration had a set of coupling constants of $\{W_2 = 30.3\,\mathrm{cm}^{-1}, W_3 = 60.7\,\mathrm{cm}^{-1}, W_4 = 59.1\,\mathrm{cm}^{-1}, W_5 = 42.1\,\mathrm{cm}^{-1}\}$, resulting in a particular value for $p(\{W_2, W_3, W_4, W_5\})$, this value would be added to the bin $W_2 = 30\,\mathrm{cm}^{-1}$, $W_3 = 61\,\mathrm{cm}^{-1}$, and so on.

By repeating this process many times, one derives a bar chart where the height of each bar corresponds to the agreement of predicted and measured overtone band integrals for this particular value of the coupling constant. Since there is no selection of which coupling constants should be sampled (like in MCMC sampling), many iterations are required and thus the name "brute-force" sampling. The result for 100M draws is compared against results from MCMC sampling in Figure S2. The results are quite similar, with the exception being the dimer, where the brute-force sampling methods suggests a very small coupling constant with the best agreement

for values even below the monomer value of about $30\,\mathrm{cm}^{-1}$. In case of the MCMC sampling, the dimer coupling constant is more spread and covers the region 0 to $75\,\mathrm{cm}^{-1}$ with maximum probability close to $30\,\mathrm{cm}^{-1}$. The coupling constants for the trimer and tetramer are very similar for both sampling methods, but for the pentamer, brute-force sampling yields overall a smaller coupling constant. However, both methods peak close to $50\,\mathrm{cm}^{-1}$.

The brute-force approach has a couple of shortcoming compared to MCMC sampling, namely that it does not yield band integral ratios (intensity ratios) directly, but coupling constants which depend on the assumptions of the simple Fermi resonance model, and that it does not handle possible bias in the measured band integrals. The former problem is that a grid for sampling intensity ratios cannot be established easily, because the intensity ratio can become very small for the dimer and trimer, on the order of a couple of percent, but be close to 1 for the tetramer and pentamer. The coupling constant, on the other hand, can be sampled with a uniform resolution of $1\,\mathrm{cm}^{-1}$ in a useful way. The later problem is due to the unselective sampling of band integrals, which is rigid and fixed to the input distributions. MCMC solves both of these problems: by sampling the input (prior) distributions selectively in the overall most probable regions it can adapt to occasional outliers in the band integrals (offending data points can be identified through the deviation of prior distribution and posterior distribution, NB/4/4.5). At the same time, it is unnecessary to define a sampling grid manually, so that the intensity ratios can be fitted directly. Further information on brute-force sampling can be found in NB/3.

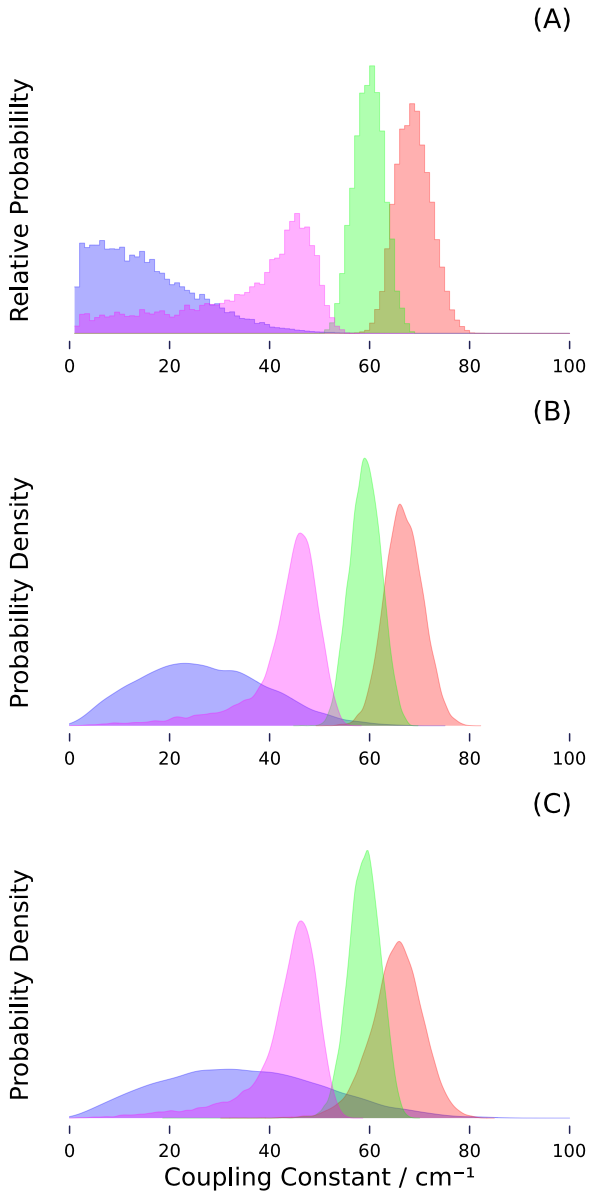

Figure S2: Comparison of coupling constants derived from brute-force and MCMC sampling. Numbers and colors indicate clusters sizes: blue - dimer, red - trimer, green - tetramer, magenta - pentamer.

References

[1] I. Bello, *Vacuum and Ultravacuum*, CRC Press, 1st edn, 2017, p. 406.

[2] D. A. Long, *The Raman Effect*, John Wiley & Sons Ltd, 2002.

[3] M. Gawrilow and M. A. Suhm, *Molecules*, 2021, **26**, 4523.

[4] H. Cybulski and J. Sadlej, *Chemical Physics*, 2007, **342**, 163–172.

[5] Analytical Methods Committee, AMCTB No. 74, *Anal. Methods*, 2016, **8**, 5553–5555.